Separation of Overlapped Non-Stationary Signals by Ridge Path Regrouping and Intrinsic Chirp Component Decomposition

Shiqian Chen, Xingjian Dong, Guanpei Xing, Zhike Peng, Wenming Zhang, *Member, IEEE*, and Guang Meng

***Abstract*— In some applications, it is necessary to analyze multi-component non-stationary signals whose components severely overlap in the time-frequency (T-F) domain. Separating those signal components is desired but very challenging for existing methods. To address this issue, we propose a novel non-parametric algorithm called ridge path regrouping (RPRG) to extract the instantaneous frequencies (IFs) of the overlapped components from a T-F representation (TFR). The RPRG first detects the ridges of a multi-component signal from a TFR and then extracts the desired IFs by regrouping the ridge curves according to their variation rates at the intersections. After the IFs are obtained, component separation is achieved by using the intrinsic chirp component decomposition (ICCD) method. Different from traditional T-F filter-based methods, the ICCD can accurately reconstruct overlapped components by using a joint-estimation scheme. Finally, applications of separating some simulated and experimental micro-Doppler signals are presented to show the effectiveness of the method.**

***Index Terms*— Multi-component signal, overlapped signals, signal decomposition, time frequency (T-F), instantaneous frequency (IF), intersected IFs, micro-Doppler (m-D).**

I. Introduction

IN MANY research fields, such as radar, mechanical engineering and bioengineering, we need to deal with non-stationary signals which have time-varying frequency contents [1]–[4]. Time-frequency (T-F) analysis methods have been widely used to capture the time-varying signatures of non-stationary signals [5]. In practice, those non-stationary signals usually contain multiple components (i.e., multi-component signals) some of which may overlap (or cross) in both time and frequency domains (e.g., the micro-Doppler (m-D) signatures [1]). Many T-F methods may fail to accurately capture all the components simultaneously. Therefore, to effectively analyze a multi-component signal, it is important to separate its signal components first [6], [7].

In the past decades, many signal decomposition methods have been proposed to obtain the constituent components of a multi-component signal. Some representative methods include: the empirical mode decomposition [8], the local mean decomposition [9], the synchrosqueezing transform [10], the empirical wavelet transform [11], the variational mode decomposition [12], the sparsification approaches [13], [14], and so on. However, most of the decomposition methods suppose that the signal components satisfy strict separation conditions in the T-F domain [10], and thus they cannot fully separate close and overlapped signal components. Recently, the intrinsic chirp component decomposition (ICCD) method proposed in [15] showed the potential of separating crossed components by using a joint-optimization technique. In essence, the ICCD acts as a T-F filter and the instantaneous frequencies (IFs) of the components (i.e., the center frequencies of the filter) should be provided in advance. However, estimating the IFs of severely overlapped components is a challenging issue for most existing methods, which prohibits the applications of the ICCD. In addition, the ICCD is developed based on the real signal model, so it cannot directly adapt to some important applications (e.g., radar signal analysis) where the signal data is complex valued.

To analyze overlapped signal components, some methods have been introduced in certain application fields. These methods can be divided into two classes, i.e., the parametric methods and the non-parametric methods. The parametric methods usually use a predefined model, such as polynomial [16]–[19], piecewise polynomial [20]–[22], and sinusoidal models [23], [24], to characterize the IFs of the components. The separation of the components can be achieved by estimating their model parameters. These methods usually involve multi-dimensional searches in the parameter space, which will be relatively time consuming. Moreover, the predefined signal model may only adapt to specific situations. In this paper, we are more interested in the non-parametric methods which are known to be more adaptive in practical applications. Such methods usually extract signatures of a multi-component signal from its time-frequency representation (TFR). In [25], the Viterbi algorithm is employed to extract IFs of signals under heavy noise. It is reported that the Viterbi algorithm can also be used to analyze overlapped signal components in [26]–[28]. Nevertheless, in reality, we find

Manuscript received July 7, 2017; revised July 29, 2017; accepted August 3, 2017. Date of publication August 8, 2017; date of current version August 22, 2017. This work was supported in part by the National Natural Science Foundation of China under Grant 11632011, Grant 11472170, and Grant 51121063, and in part by the Technology Innovation Program of Advanced Aerospace Technology Joint Center under Grant USCAST2016-26. The associate editor coordinating the review of this paper and approving it for publication was Prof. Aime Lay-Ekuakille. *(Corresponding author: Zhike Peng.)*

S. Chen, X. Dong, Z. Peng, W. Zhang, and G. Meng are with the State Key Laboratory of Mechanical System and Vibration, Shanghai Jiao Tong University, Shanghai 200240, China (e-mail: chenshiqian@sjtu.edu.cn; donxij@sjtu.edu.cn; z.peng@sjtu.edu.cn; wenmingz@sjtu.edu.cn; gmeng@sjtu.edu.cn).

G. Xing is with the Shanghai Aerospace Electronic Technology Institute, Shanghai 201109, China (e-mail: xingguanpei@163.com).

Digital Object Identifier 10.1109/JSEN.2017.2737467

that this algorithm may track wrong IFs for some seriously intersecting components. In addition, the computational complexity of the algorithm is relatively high because it needs to search many candidate paths in the T-F plane. In [29]–[31], the L- statistic of a TFR is adopted to separate stationary and non-stationary components of a multi-component signal. Other works sharing similar goals can be found in [32]–[34]. These methods only obtain the non-stationary parts of the signal. They cannot further decompose the non-stationary components. Image processing techniques can also be used to estimate IFs of a multi-component signal from a TFR, as shown in [35]. However, this approach is computationally prohibitive in practical applications since it needs an exhaustive search.

One can find that separating overlapped components is still a challenging task for the methods mentioned above. To address this issue, we propose a fully non-parametric method which can be applied to a wide range of signals. The proposed method first indentifies overlapped components (from a TFR) using a novel algorithm called ridge path regrouping (RPRG) and then separates these components by the ICCD. The RPRG includes two steps: 1) detect ridges (i.e., local maximum values) of a TFR for a multi-component signal; 2) regroup the obtained ridge curves according to their variation rates at the intersection points. The RPRG is efficient (it does not involve exhaustive searches) and can effectively extract the IFs of overlapped components. In addition, we extend the ICCD in [15] to process complex-valued data and present an application of separating overlapped m-D signals.

Our paper is organized as follows. In Section II, after a brief introduction of the signal model, we describe how to deal with the complex-valued signal by ICCD. In Section III, the limitations of current ridge detection methods are discussed first, and then the RPRG algorithm is detailed. Simulation results of separating some m-D signals are provided in Section IV. We draw the conclusions in Section V.

II. Background

A. Signal Model and T-F Representation

Consider a multi-component non-stationary signal contaminated by a white Gaussian noise as

$$x(t) = \sum_{m=1}^{M} x_m(t) + \eta(t) = \sum_{m=1}^{M} a_m(t)\, e^{j\left[2\pi \int_0^t IF_m(r)dr + \varphi_m\right]} + \eta(t) \quad (1)$$

where M is the number of the components, $j = \sqrt{-1}$, $a_m(t) \in C^1(\mathbb{R}) > 0$ is the amplitude function, $IF_m(t) \in C^1(\mathbb{R})$ denotes the instantaneous frequency (IF), φ_m is the initial phase, $\eta(t)$ represents the noise. The amplitude and the frequency of the components are slowly varying functions such that $\left|a'_m(t)\right|, \left|IF'_m(t)\right| \ll |IF_m(t)|$. The complex signal model in (1) is widely used in practical applications such as radar. In fact, the real and imaginary parts of the radar signal come from two quadrature (I/Q) channels which can be used to determine the direction of target motion.

It is worth noting that many methods are developed under the separation conditions of the components: $IF_m(t) < IF_{m+1}(t)$ $(m = 1, \cdots, M)$. In this paper, we deal with the challenging case that there exist components overlapping in the time-frequency (T-F) domain. We provide the following definition:

Definition 1: The two components $x_k(t)$ and $x_m(t)$ in model (1) are said to cross (or overlap) in the T-F domain if there exist a time instant $\bar{t}_{k,m}$ and a bound $d > 0$ such that their IFs satisfy:

$$IF_k\left(\bar{t}_{k,m}\right) = IF_m\left(\bar{t}_{k,m}\right), \quad (2)$$

$$\left|IF'_k\left(\bar{t}_{k,m}\right) - IF'_m\left(\bar{t}_{k,m}\right)\right| \geq d. \quad (3)$$

Formula (3) indicates that the IFs of the two components have different variation rates at the intersecting time $\bar{t}_{k,m}$. It is the basis of identifying these overlapped components for our algorithm in Section III. The parameter d controls the difference of the variation rates. When d is larger, it will be easier to discriminate these components. Note that we do not consider the case that the two components are tangent to each other (i.e., $IF'_k\left(\bar{t}_{k,m}\right) = IF'_m\left(\bar{t}_{k,m}\right)$) since it is difficult to tell these components apart according to their geometry in the T-F domain.

To effectively capture the time-varying frequency contents of model (1), the T-F representation (TFR) of the signal can be obtained by certain T-F transforms. The short-time Fourier transform (STFT) is one of the most widely used methods and defined as

$$TF(t, f) = \int_{\mathbb{R}} x(\tau)\, g_\sigma(\tau - t)\, e^{-j2\pi f \tau} d\tau \quad (4)$$

where $TF(t, f)$ is the obtained TFR, $g_\sigma(\tau)$ is a Gaussian window with length of σ. The IFs of the signal can be extracted from the TFR, which will be illustrated in Section III.

B. Extended Intrinsic Chirp Component Decomposition

The intrinsic chirp component decomposition (ICCD) method originally proposed in [15] can only be used to analyze real-valued data. In this section, the ICCD is extended to process the complex signal model in (1). Supposing that the signal is observed in discrete time $t = t_0, \cdots, t_{N-1}$, the formula (1) can be arranged as

$$x(t) = \sum_{m=1}^{M} \bar{a}_m(t)\, e^{j2\pi \int_0^t IF_m(r)dr} + \eta(t), \quad t = t_0, \cdots, t_{N-1} \quad (5)$$

where $\bar{a}_m(t) = a_m(t)\, e^{j\varphi_m}$ is a complex envelope. Note that $\bar{a}_m(t)$ is a smooth function which can be characterized by Fourier basis as:

$$\bar{a}_m(t) = a_0^{(m)} + \sum_{k=1}^{K} a_k^{(m)} \cos\left(2k\pi \bar{f}_0 t\right) + b_k^{(m)} \sin\left(2k\pi \bar{f}_0 t\right) \quad (6)$$

where $a_0^{(m)}, \cdots, a_K^{(m)}, b_1^{(m)}, \cdots, b_K^{(m)}$ are complex Fourier coefficients; $\bar{f}_0 = F_s/QN$ is the base frequency, where Q is

a positive integer, F_s is the sampling frequency. To better represent non-periodic functions, we let $Q > 1$ (e.g., $Q = 2$ in this paper) to obtain a redundant Fourier basis [14]. Now inserting (6) into (5) leads to the following equation

$$\boldsymbol{x} = \boldsymbol{G}\boldsymbol{p} + \boldsymbol{n} \tag{7}$$

where $\boldsymbol{x} = [x(t_0)\cdots x(t_{N-1})]^T$, $\boldsymbol{n} = [\eta(t_0)\cdots\eta(t_{N-1})]^T$, $\boldsymbol{p} = [(\boldsymbol{p}_1)^T\cdots(\boldsymbol{p}_M)^T]^T$ with $\boldsymbol{p}_m = [a_0^{(m)}\cdots a_K^{(m)}\ b_1^{(m)}\cdots b_K^{(m)}]^T$ (herein the superscript $(\cdot)^T$ denotes transposition), $\mathbf{G} = [\mathbf{G}_1\cdots\mathbf{G}_M]$. The sub-matrix $\mathbf{G}_m$ is of size $N \times (2K+1)$ whose elements can be obtained as (for $c = 1,\cdots,N$, $d = 1,\cdots,2K+1$):

$$(\mathbf{G}_m)_{cd} = \begin{cases} e^{j\psi(t_{c-1})}\cdot\cos[2(d-1)\pi\,\bar{f}_0 t_{c-1}], & d \in [1, K+1] \\ e^{j\psi(t_{c-1})}\cdot\sin[2(d-K-1)\pi\,\bar{f}_0 t_{c-1}], & d \in [K+2, 2K+1] \end{cases} \tag{8}$$

where $\psi(t) = 2\pi\int_0^t IF_m(r)\,dr$.

To estimate the unknown coefficients, the following optimization problem should be addressed:

$$\bar{\boldsymbol{p}} = \arg\min_{p}\left\{\|\boldsymbol{x} - \mathbf{G}\boldsymbol{p}\|^2 + \alpha\,\|\boldsymbol{p}\|^2\right\} \tag{9}$$

where $\|\cdot\|$ stands for the Euclidean norm, $\alpha\,\|p\|^2$ is the Tikhonov regularization term for the ill-posed problem. The solution of (9) can be easily obtained as

$$\bar{\boldsymbol{p}} = \left(\mathbf{G}^H\mathbf{G} + \alpha\mathbf{I}\right)^{-1}\mathbf{G}^H\boldsymbol{x} \tag{10}$$

where $(\cdot)^H$ denotes the conjugate transpose of a complex matrix. Generally, the parameter α is chosen to be proportional to the noise level. There are many effective methods available for finding a good α, such as the L-curve method in [36]. In practice, the solution is not sensitive to α for our problem. Therefore, it is easy for one to empirically find an acceptable α according to the prior information (for example, we let $\alpha = 5$ for the results in Section IV). After obtaining the coefficient vector by (10), each signal component can be reconstructed as

$$\bar{\boldsymbol{x}}_m = \mathbf{G}_m\bar{\boldsymbol{p}}_m \tag{11}$$

where $\bar{\boldsymbol{p}}_m$ is a sub-vector (of Eq. (10)) composed of the estimated coefficients of the m-th component. Note that, using the estimated coefficients, the complex amplitude $\bar{a}_m(t)$ can be extracted by (6). Then, the amplitude function in (1) can be estimated by taking the modulus as $a_m(t) = |\bar{a}_m(t)|$.

The proposed new version of the ICCD above can be used to analyze complex-valued data (e.g., the m-D signals in Section IV). In fact, the ICCD can be regarded as a T-F filter, as shown in Fig. 1. Its center frequency is the IF (i.e., $IF_m(t)$) of the signal component which should be specified by the user (so that the matrix $\mathbf{G}_m$ in (8) can be obtained). Its bandwidth is determined by the Fourier order K in (6) as:

$$\text{Bandwidth} = 2K\,\bar{f}_0. \tag{12}$$

Clearly, the pass band of the filter is $[IF_m(t) - K\bar{f}_0,\ IF_m(t) + K\bar{f}_0]$. The filter can accurately extract the components in the pass-band.

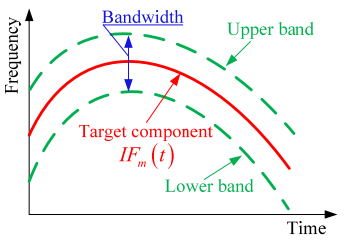

Fig. 1. Illustration of the ICCD.

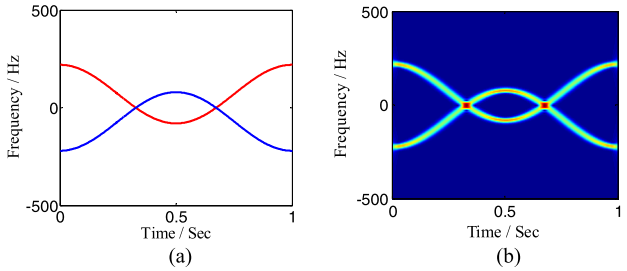

Fig. 2. A two-component signal used for illustration of ICCD. (a) Theoretical IFs. (b) TFR.

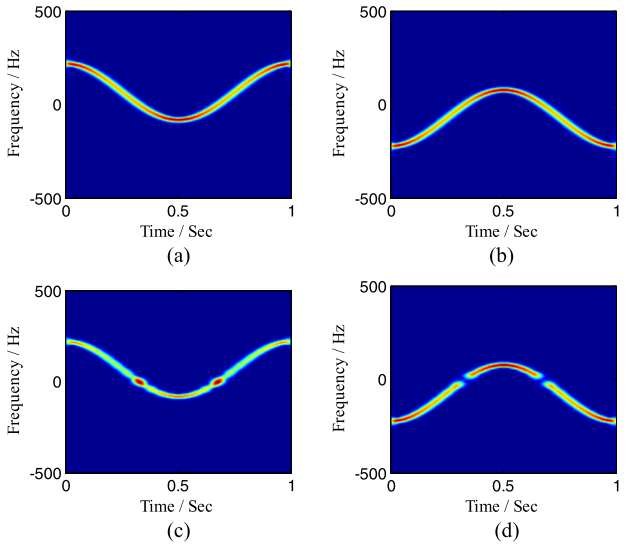

Fig. 3. Component separation by ICCD and traditional T-F filter for the test signal in Fig. 2 (herein the theoretical IFs of the two components are supposed to be known). (a) and (b) The TFRs of the two extracted components by ICCD. (c) and (d) The results by traditional T-F filter.

It can be seen that the ICCD concurrently extracts all the components by solving the joint-optimization problem in (9). As a result, the ICCD can fully separate overlapped components [15]. On the other hand, traditional T-F filter only extracts one component in one execution [19]–[21], [28]. The first extracted component often contains more than enough information (i.e., the involvement of other components) at the crossing points. A two-component signal with crossed IFs (see Fig. 2) is considered to show the advantage of ICCD. In this paper, without special note, the TFRs of signals are obtained by STFT with window length of 128 samples (e.g., Fig. 2(b)). The component separation results by ICCD and traditional T-F filter are shown in Fig. 3 where the

bandwidth is set to 40 Hz for both methods. It can be seen that the ICCD can fully (or accurately) separate the overlapped components (see Fig. 3(a) and (b)) because the simultaneous-estimation scheme in (9) can balance the energy of the components at the crossing points. However, for the traditional T-F filter, it is shown that the first extracted component (see Fig. 3(c)) takes away partial energy of the other component (see Fig. 3(d)) at the intersections. This example indicates that the ICCD can be employed to separate crossed components in practical applications. To do so, we need to address a very important but challenging issue that how to extract IFs of crossed components for the ICCD. In next section, our solution will be presented.

III. IF Extraction by Ridge Path Regrouping

A. Limitations of Current Methods

The IF can be estimated by detecting ridges from a TFR. This method is fully non-parametric and adaptive to different situations. An efficient ridge detection method is to find maxima positions of a TFR as [37]

$$\overline{IF}(t) = \arg\max_{f \in F} |TF(t, f)|, \quad t = t_0, \cdots, t_{N-1} \tag{13}$$

where $\overline{IF}(t)$ denotes the obtained ridge curve which is an estimate of the theoretical IF $IF(t)$, $\mathbf{F}$ is the set of frequency bins, the signal is supposed to be measured in discrete time $t = t_0, \cdots, t_{N-1}$. However, this method may find positions caused by noise in a noisy environment or those of other components for a multi-component signal. Some more effective methods try to find a smooth ridge curve which goes through positions with large energies of the TFR as [38]:

$$\overline{IF}(t) = \arg\max_{\Omega(t) \in \mathbf{\Theta}} \left\{ \sum_{l=0}^{N-1} |TF(t_l, \Omega(t_l))|^2 - \lambda \sum_{l=1}^{N-1} |\Omega(t_l) - \Omega(t_{l-1})| \right\} \tag{14}$$

where $\mathbf{\Theta}$ denotes the set of all the possible paths at $t = t_0, \cdots, t_{N-1}$, λ is a penalty parameter which regulates the variation degree of the obtained ridge curve (at two consecutive points). The method (14) needs to search many paths in the T-F plane, which is computationally prohibitive. Some dynamic programming algorithms such as the Viterbi algorithm [25] have been employed to solve the difficult task, but the computational cost is still too high. Herein a tractable algorithm sharing the similar idea of (14) [39], [40] is introduced in Algorithm 1 where Δf denotes the maximum allowable frequency variation between two consecutive points. Note that, for a multi-component signal, the methods introduced above will first extract the ridge curve of the strongest component, denoted by $\overline{IF}_1(t)$. After masking the extracted component in the T-F domain (e.g., by setting $TF(t, f)$ to zeros around $\overline{IF}_1(t)$), the ridge curves of components with smaller energies can be extracted by repeating these methods.

It can be found that the current methods introduced above may fail to extract IFs of overlapped components for two reasons: 1) these methods extract IFs only based on the magnitudes and the absolute frequency variations without considering the variation directions of the ridge curves; 2) these methods try to extract smooth ridge curves by only limiting the frequency variations of two consecutive sampling points, which is not strong enough to resolve overlapped components (the sampling interval is too small and thus the constraint in the interval is local and weak). To show the limitation, an example is provided in Fig. 4 where $IF_k(t)$ and $IF_m(t)$ are IFs of the two overlapped components; points 1∼14 stand for obtained ridge points; Δf_m and Δf_k denote the frequency variations of points 6, 11 and points 6, 7, respectively. It can be seen that ridge points 1∼10 are the desired ones for estimating $IF_k(t)$. However, when $\Delta f_k \approx \Delta f_m$ and points 11∼14 have larger magnitudes than those of points 7∼10, the current methods will find ridge points 1∼6, 11∼14 for $IF_k(t)$ (see Fig. 4). This example indicates that the current methods cannot properly identify overlapped components. To address this problem, one may add stronger (global) constraints in formula (14). Nevertheless, as mentioned before, solving the resulting optimization problem is computationally prohibitive. In next subsection, we will introduce a simple and efficient method called ridge path regrouping (RPRG) to deal with this challenging task.

Algorithm 1 Ridge detection

Input: Δf

1: Find $(t_m, f_m) = \arg\max_{t,f} |TF(t, f)|$ and let $\overline{IF}(t_m) = f_m$, $\bar{f}_R = f_m$, $\bar{f}_L = f_m$.

2: **for** $r = m+1, m+2, \cdots, N-1$ and $l = m-1, m-2, \cdots, 0$ **do**

3: Find $\bar{f}_R = \arg\max_{f \in [\bar{f}_R - \Delta f, \bar{f}_R + \Delta f]} |TF(t_r, f)|$ and let $\overline{IF}(t_r) = \bar{f}_R$.

4: Find $\bar{f}_L = \arg\max_{f \in [\bar{f}_L - \Delta f, \bar{f}_L + \Delta f]} |TF(t_l, f)|$ and let $\overline{IF}(t_l) = \bar{f}_L$.

5: **end for**

Output: $\overline{IF}(t)$ for $t = t_0, \cdots, t_{N-1}$

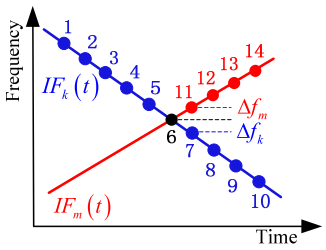

Fig. 4. Detected possible ridge points for estimating $IF_k(t)$.

B. Ridge Path Regrouping

The existing methods only focus on detecting the ridge curve of the target component without considering ridge patterns of other components. In fact, if the ridge information of other components is available, identifying the target component will become much easier. Therefore, our method

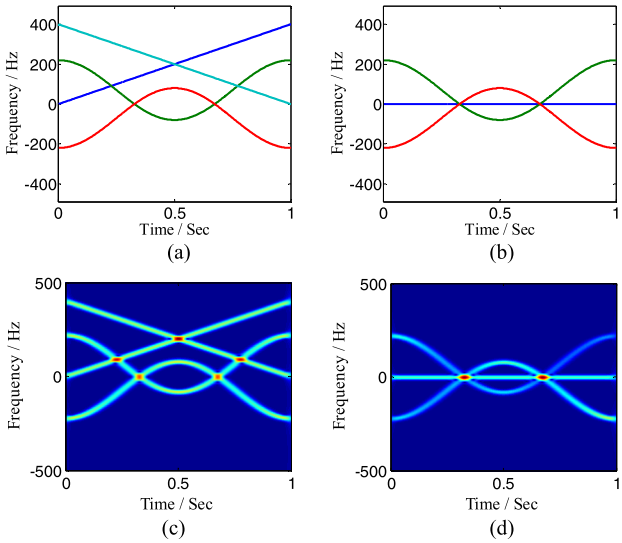

Fig. 5. Two signals used for illustration of RPRG. (a) and (b) The theoretical IFs of the two signals. (c) and (d) The TFRs of the signals.

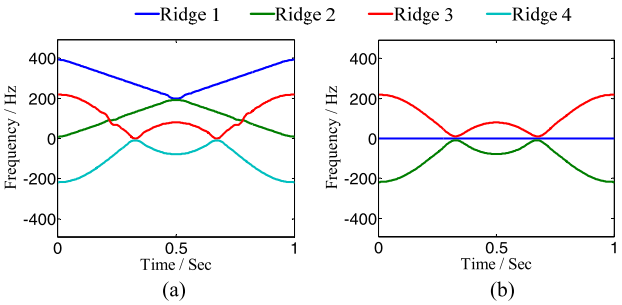

Fig. 6. Detected ridges for the two signals in Fig. 5 by Algorithm 1 (herein the ridges are numbered as 1, 2, 3, and 4).

exploits the ridge patterns of all the components simultaneously. Specifically, the proposed RPRG algorithm is developed based on the observation that:

$$\bigcup_{m=1}^{M} \overline{IF}_m(t) \approx \bigcup_{m=1}^{M} IF_m(t) \tag{15}$$

where M is the number of the components which is supposed to be known in this paper, $\overline{IF}_m(t)$ denotes the detected ridge curve by current methods (e.g., Algorithm 1), $IF_m(t)$ is the true IF. Equation (15) means that although an individual ridge curve $\overline{IF}_m(t)$ may not match any component (e.g., the example in Fig. 4), all the ridge curves as a whole can reflect the global T-F patterns of a multi-component signal. To clearly show this observation, we consider two signals in Fig. 5 and extract the ridge curves of the two signals by Algorithm 1 as shown in Fig. 6. It can be seen that, for overlapped components, some individual ridge curves track wrong components after the crossing points (e.g., see the blue and red curves in Fig. 6(a)) but all the obtained ridges can clearly reveal global T-F signatures of all the components. The basic idea of the proposed RPRG algorithm is to extract the desired IFs by regrouping the obtained ridges at the intersections. The whole procedures of the RPRG will be introduced in the following paragraphs.

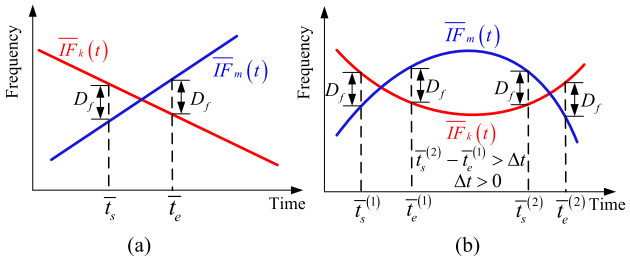

Fig. 7. Illustration of intersection intervals for two overlapped ridge curves. (a) Case with only one interval. (b) Case with multiple intervals.

Step 1: Calculate the TFR $TF(t, f)$ of the M-component signal and detect all the ridges from the TFR by Algorithm 1. In this paper, the STFT in (4) is used to generate the TFR for its simple implementation. For Algorithm 1, it is suggested to set Δf to 3% of the sampling frequency according to our experiments. Generally, if specifying a small Δf, the algorithm will find a smooth ridge curve but may fail to capture some fast varying IFs. On the other hand, the algorithm may be less robust to the disturbance of noise with a relatively large Δf [40]. In practice, one should balance the tradeoff between the two cases. The obtained ridge curves are denoted by $\overline{IF}_1(t), \cdots, \overline{IF}_M(t)$. Note that the ridge curves are only observed in discrete time (e.g., see Algorithm 1).

Step 2: Find all the intersection intervals for arbitrary two overlapped ridge curves as shown in Fig. 7. To do so, we provide the following definition:

Definition 2: Assuming that $\bar{t}_s, \bar{t}_e$ are two sampling instants, the time interval $[\bar{t}_s, \bar{t}_e]$ is said to be an intersection interval (with a small separation distance of D_f) of the two ridge curves $\overline{IF}_k(t)$ and $\overline{IF}_m(t)$ if the following conditions are satisfied:

$$\left|\overline{IF}_k(t) - \overline{IF}_m(t)\right| \le D_f, \quad \text{for } t \in [\bar{t}_s, \bar{t}_e] \tag{16}$$

$$\left|\overline{IF}_k(t) - \overline{IF}_m(t)\right| > D_f, \quad \text{for } t = \bar{t}_s - 1/F_s \text{ and } t = \bar{t}_e + 1/F_s \tag{17}$$

where D_f is a predefined threshold; $\bar{t}_s$, $\bar{t}_e$ stand for the starting and ending time of the interval, respectively; F_s is the sampling frequency. Note that, due to the ridge detection errors, the extracted rides of some intersecting signal components may not intersect. That is, there may exist a small separation distance between such rides (e.g., see the red and green ridge curves in Fig. 11(b)). Therefore, in *Definition 2*, a threshold D_f is considered to find such intersection intervals. The threshold D_f controls the length of the intersection interval, i.e., $\left|\bar{t}_e - \bar{t}_s\right|$. Obviously, if D_f is larger, the interval length will become larger. In fact, due to the severe interference of different components, there often exist larger errors for the detected ridges near the intersections (e.g., see Fig. 6(a)). Therefore, the ridges in the intersection interval will be discarded and we will generate new ridge segments in the interval by interpolation method (see details latter in Step 4). Accordingly, if specifying a too large D_f, some good ridges will also be discarded, and the ridge interpolation (in a long interval) will introduce large errors. On the contrary, if D_f is very small, some rough ridges will still be retained, and sometimes some intersection

intervals will not be identified. In this paper, D_f is set to 3% of the sampling frequency which provides a good balance of the two cases according to our simulation tests. It is worth noting that there may exist multiple intersection intervals for two ridge curves (e.g., the intervals $\left[\bar{t}_s^{(1)}, \bar{t}_e^{(1)}\right]$ and $\left[\bar{t}_s^{(2)}, \bar{t}_e^{(2)}\right]$ in Fig. 7(b)). It is assumed that two different intervals are separable (e.g., $\bar{t}_s^{(2)} - \bar{t}_e^{(1)}$ is larger than a time increment Δt in Fig. 7(b)) and thus can be identified in the time axis. All the intersection intervals of the obtained ridge curves can be found according to *Definition 2*. For algorithmic simplicity, we number these intersection intervals and express the i-th interval as

$$\mathbf{\Lambda}^{(i)} = \left[\mathbf{R}^{(i)}, \mathbf{T}^{(i)}\right] = \left[\left\{R_1^{(i)}, R_2^{(i)}\right\}, \left\{\bar{t}_s^{(i)}, \bar{t}_e^{(i)}\right\}\right] \quad (18)$$

where $\mathbf{R}^{(i)} = \{R_1^{(i)}, R_2^{(i)}\} \subseteq \{1, \cdots, M\}$ denotes the set of the (overlapped) ridge numbers (i.e., the two ridges $\overline{IF}_{R_1^{(i)}}(t)$ and $\overline{IF}_{R_2^{(i)}}(t)$ overlap in this interval); $\mathbf{T}^{(i)} = \{\bar{t}_s^{(i)}, \bar{t}_e^{(i)}\}$ is the set of the starting and ending time instants of the interval. For example, one can find five intersection intervals for the ridges in Fig. 6(a) (see Fig. 8(a)) and these intervals are denoted by $[\{2, 3\}, \{0.205, 0.255\}]$, $[\{3, 4\}, \{0.306, 0.353\}]$, $[\{1, 2\}, \{0.461, 0.543\}]$, $[\{3, 4\}, \{0.650, 0.697\}]$, and $[\{2, 3\}, \{0.747, 0.798\}]$, respectively. All these intersection intervals clearly describe the connection relations of these ridges.

Step 3: Merge intersection intervals which are close to each other in the T-F plane. In Step 2 above, all the intersection intervals belonging to arbitrary two overlapped ridges were obtained. In some challenging cases, however, the number of the ridges presenting at an intersection point (i.e., the number of the elements in set $\mathbf{R}^{(i)}$ in (18)) may be larger than two. Therefore, some of the intersection intervals obtained by *Definition 2* may be redundant. For example, the three ridge curves in Fig. 6(b) only have two intersection points but we will find six intersection intervals for arbitrary two ridge curves according to *Definition 2*. To address this issue, we propose to merge some close and overlapped intervals. First, the distance of arbitrary two intersection intervals in the T-F plane should be detected, denoted by $\text{dist}\left(\mathbf{\Lambda}^{(i)}, \mathbf{\Lambda}^{(q)}\right)$. If $\text{dist}\left(\mathbf{\Lambda}^{(i)}, \mathbf{\Lambda}^{(q)}\right) \le D_{t-f}$ where D_{t-f} is a threshold, the two intervals will be merged as:

$$\mathbf{\Lambda}^{(i)} \oplus \mathbf{\Lambda}^{(q)} = \left[\mathbf{R}^{(i)} \cup \mathbf{R}^{(q)}, \left\{\min\left(\mathbf{T}^{(i)} \cup \mathbf{T}^{(q)}\right), \max\left(\mathbf{T}^{(i)} \cup \mathbf{T}^{(q)}\right)\right\}\right] \quad (19)$$

where the symbol $\oplus$ stands for the defined merging operation. If we denote the cardinality (i.e., the number of the elements) of the set $\mathbf{R}^{(i)}$, $\mathbf{R}^{(q)}$ by $I = \text{card}\left(\mathbf{R}^{(i)}\right)$ and $Q = \text{card}\left(\mathbf{R}^{(q)}\right)$, the distance of two intersection intervals can be defined as:

$$\text{dist}\left(\mathbf{\Lambda}^{(i)}, \mathbf{\Lambda}^{(q)}\right) = \sqrt{\left(\bar{t}_e^{(i)} - \bar{t}_e^{(q)}\right)^2 + \left[\sum_{k=1}^{I} \overline{IF}_{R_k^{(i)}}\left(\bar{t}_e^{(i)}\right)/I - \sum_{k=1}^{Q} \overline{IF}_{R_k^{(q)}}\left(\bar{t}_e^{(q)}\right)/Q\right]^2} \quad (20)$$

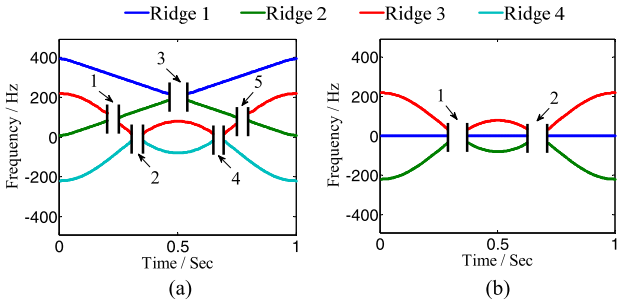

Fig. 8. Intersection intervals of the ridges in Fig. 6 (the ridges in the intersection intervals are not plotted).

which is essentially the Euclidean distance of the two T-F points $\left(\bar{t}_e^{(i)}, \sum_{k=1}^{I} \overline{IF}_{R_k^{(i)}}\left(\bar{t}_e^{(i)}\right)/I\right)$ and $\left(\bar{t}_e^{(q)}, \sum_{k=1}^{Q} \overline{IF}_{R_k^{(q)}}\left(\bar{t}_e^{(q)}\right)/Q\right)$. Generally, the distance (calculated by (20)) of the intersection intervals belonging to the same intersection point is very small. Therefore, one can easily find a proper threshold D_{t-f} to identify them. According to our tests, it is suggested the distance threshold $D_{t-f} = \gamma D_f$ where D_f is defined in *Definition 2*, $1 \le \gamma \le 2$ is a proportionality coefficient (i.e., D_{t-f} is slightly larger than D_f; in the paper, we let $\gamma = 2$). One should repeat the merging operation in (19) until the distance of arbitrary two intersection intervals is larger than D_{t-f}. For example, after the merging operation, we only obtain two intersection intervals for the ridges in Fig. 6(b) (see Fig. 8(b)) which are denoted by $[\{1, 2, 3\}, \{0.288, 0.374\}]$ and $[\{1, 2, 3\}, \{0.628, 0.717\}]$. As shown in Fig. 8, the intersection intervals are sorted according to the ascending order of the ending time of each interval (i.e., $\bar{t}_e^{(i)} < \bar{t}_e^{(i+1)}$).

Step 4: Regroup ridges in each intersection interval. To do so, the detected ridge curves are broken first and then reconnected according to the variation rates of the ridge curves in the intervals. It is obvious that the time axis is divided into three segments by an intersection interval $\mathbf{\Lambda}^{(i)}$ as $\left(-\infty, \bar{t}_s^{(i)}\right]$, $\left(\bar{t}_s^{(i)}, \bar{t}_e^{(i)}\right)$ and $\left[\bar{t}_e^{(i)}, +\infty\right)$. In this paper, we break the ridge curves by discarding original ridge segments in $\left(\bar{t}_s^{(i)}, \bar{t}_e^{(i)}\right)$ where new ridges will be generated to correctly connect the ridge curves in $\left(-\infty, \bar{t}_s^{(i)}\right]$ and $\left[\bar{t}_e^{(i)}, +\infty\right)$, as illustrated in Fig. 9. The most important task is to redefine the correct connection relations of the ridges in the intersection interval. To this end, the slopes (or variation rates) of the ridges at the time instants $\bar{t}_s^{(i)}$ and $\bar{t}_e^{(i)}$ can be approximately obtained as:

$$slp^{-}_{R_k^{(i)}} = \left[\overline{IF}_{R_k^{(i)}}\left(\bar{t}_s^{(i)}\right) - \overline{IF}_{R_k^{(i)}}\left(\bar{t}_s^{(i)} - \Delta t\right)\right]/\Delta t \quad (21)$$

$$slp^{+}_{R_k^{(i)}} = \left[\overline{IF}_{R_k^{(i)}}\left(\bar{t}_e^{(i)} + \Delta t\right) - \overline{IF}_{R_k^{(i)}}\left(\bar{t}_e^{(i)}\right)\right]/\Delta t \quad (22)$$

where $\Delta t > 0$ is a small time increment. Mathematically, Δt should be sufficiently small. However, in practice (i.e., in discrete time cases), the obtained slopes may not be stable and cannot properly reflect the trend of the ridge

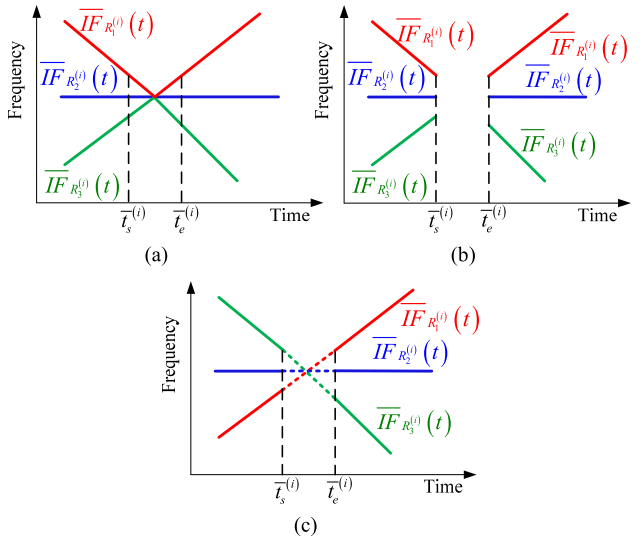

Fig. 9. Illustration of ridge regrouping procedures for the i-th intersection interval (this example has three ridge curves overlapping in the interval). (a) Detected ridge curves. (b) Ridge breaking. (c) Ridge reconnection (through interpolation).

curves with a too small Δt under the disturbance of noise. In this paper, Δt is set to 1.5% of the time duration of the signal. In reality, we find the performance of the method is not sensitive to Δt. Therefore, the parameter can be fixed to the suggested value for a wide range of applications. Then a connection matrix which measures the matching degree of different ridge segments in $\left(-\infty, \bar{t}_s^{(i)}\right]$ and $\left[\bar{t}_e^{(i)}, +\infty\right)$ is defined as:

$$CM^{(i)}(m,n) = \left| slp^{-}_{R_m^{(i)}} - slp^{+}_{R_n^{(i)}} \right|, \quad m,n = 1,\cdots,I \tag{23}$$

where I is the number of the intersecting ridge curves in the interval $\mathbf{\Lambda}^{(i)}$. The correct connection pair can be determined by finding the minimum element of the matrix as:

$$(m_0, n_0) = \underset{m,n\in\{1,\cdots,I\}}{\arg\min} \; CM^{(i)}(m,n) \tag{24}$$

which means that the ridge segments $\overline{IF}_{R_{m_0}^{(i)}}(t)$ in $\left(-\infty, \bar{t}_s^{(i)}\right]$ and $\overline{IF}_{R_{n_0}^{(i)}}(t)$ in $\left[\bar{t}_e^{(i)}, +\infty\right)$ should be connected in this intersection interval because they have similar variation rates. To connect the two ridge segments, we linearly interpolate the ridge between the two T-F points $\left(\bar{t}_s^{(i)}, \overline{IF}_{R_{m_0}^{(i)}}\left(\bar{t}_s^{(i)}\right)\right)$ and $\left(\bar{t}_e^{(i)}, \overline{IF}_{R_{n_0}^{(i)}}\left(\bar{t}_e^{(i)}\right)\right)$ (e.g., see Fig. 9(c)). In fact, one may choose higher-order interpolations. But it does not significantly improve the result according to our experiments. Having found the first connection pair, all the elements of the m_0-th row and the elements of the n_0-th column of the matrix $CM^{(i)}$ should be set to sufficiently large values (e.g., $+\infty$). Then, we can repeat (24) and the above procedure to connect other ridge segments in this interval. Furthermore, the ridge regrouping algorithm above should be repeated for all the intersection intervals to extract the correct ridge curves

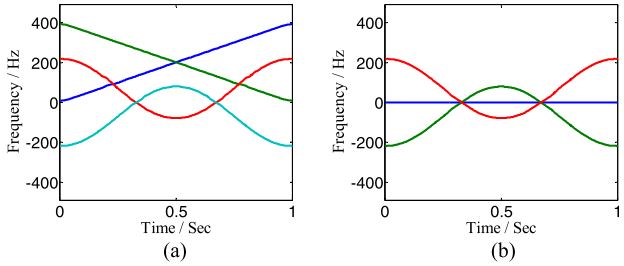

Fig. 10. Extracted IFs by the RPRG for the two signals in Fig. 5.

(or IFs) of the components. Fig. 10 provides the extracted IFs by the proposed method for the signals in Fig. 5.

The IF information of overlapped components can be extracted by the RPRG algorithm presented above. In addition, one can find that the RPRG does not involve exhaustive searches and thus is computationally efficient. For example, to obtain the results in Fig. 10 (a) and (b), the RPRG (including steps of calculating TFR of the signal, detecting ridges from the TFR and regrouping ridges) requires about 0.4 s and 0.3 s, respectively, which is acceptable for many applications. Using the IF information, we can separate the overlapped components by the ICCD introduced in Section II-B. In the following section, some numerical results will be provided to show the effectiveness of the proposed method.

IV. Validation

It is known that m-D effect has been widely used for target recognition and detection in radar systems [41], [42]. Generally, the m-D signals from multiple moving targets (or from multiple scattering points of the same target) may severely overlap in the T-F domain. To accurately extract m-D signatures, it is important to decouple these overlapped signal components first. In this section, the proposed method will be applied to separate both simulated and experimental m-D signals. Hereinafter, to quantify the noise level of the observed signal or the accuracy of the estimated signal by the proposed method, the signal to noise ratio (SNR; unit: dB) is calculated as

$$\mathrm{SNR} = 10\log_{10}\left(\frac{\|x(t)\|^2}{\|\tilde{x}(t) - x(t)\|^2}\right) \tag{25}$$

where $\|\cdot\|$ denotes the l_2 norm, $x(t)$ is the true signal, $\tilde{x}(t)$ stands for the observed (noisy) or estimated signal.

A. Simulation Results

In this subsection, the m-D induced by some typical moving targets, i.e., rotating, tumbling, and coning targets [1] will be considered. First, we consider a rotating target with four strong scattering points, i.e., three rotating points and one stationary point at the center of rotation. The rotation radius of the rotating points is 6.5 m and the angular velocity is 4π rad/s. Herein it is assumed that the wavelength of the radar waves is 0.06 m. A Gaussian white noise is artificially added to the resulting m-D signal and the SNR is 0 dB, as shown in Fig. 11(a). It can be seen that the m-D signatures of the

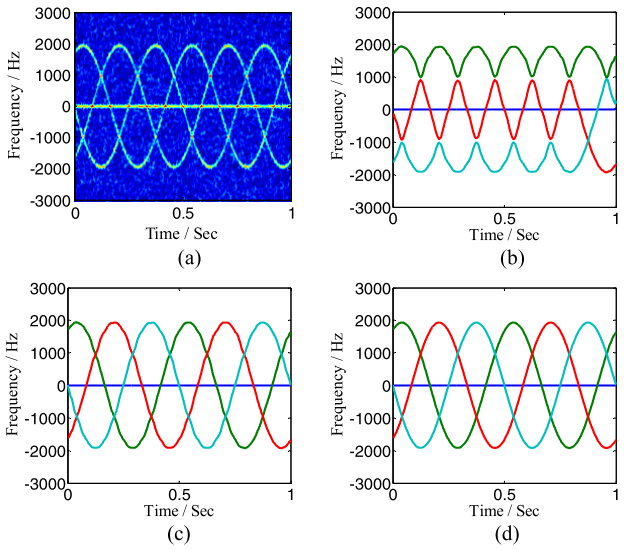

Fig. 11. Simulated m-D signal of a rotating target and the IF extraction results. (a) TFR of the noisy m-D signal (SNR = 0 dB). (b) Result by ridge detection. (c) Result by RPRG. (d) Result after smoothing the curves in (c).

three rotating points are sinusoidal curves while that of the stationary point is a horizontal line at zero frequency. The detected ridge curves from the TFR of the signal are provided in Fig. 11(b). It shows that the traditional ridge detector cannot track correct IFs for the m-D signal with severely overlapped components. On the other hand, the proposed RPRG algorithm can effectively identify these crossed components by considering the variation rates of the ridge curves, as shown in Fig. 11(c). To reduce the interference of the noise, one can further smooth the extracted IFs by least-squares fitting with a Fourier model (e.g., the model in (6)), as illustrated in Fig. 11(d). Having extracted the IFs, we can separate the components of the m-D signal by ICCD as shown in Fig. 12. It shows that all the components are successfully extracted and the SNR is significantly improved.

Next, we consider the m-D of a tumbling target which has an initial velocity of 5 m/s along the horizontal direction, an acceleration of 9.8 m/s^2 caused by the gravity, and also rotates with an angular velocity of 4π rad/s [1]. It is assumed that the target has three strong scattering points one of which is located at the center of the rotation. The m-D signal is also contaminated by strong white noise and the SNR is 0 dB, as shown in Fig. 13(a). It can be seen that the m-D signatures of the two rotating points are no longer the standard sinusoidal curves (i.e., oscillating around the zero) due to the gravity. Therefore, the parametric methods which employ sinusoidal models cannot directly adapt to this situation. The IF extraction results for the signal are shown in Fig. 13(b)∼(d). Comparing with the result by traditional ridge detector (see Fig. 13(b)), the proposed method can not only track the correct ridge paths for the overlapped components but also reduce the errors of the ridges near the intersection points through ridge interpolation (see Fig. 13(c)). The component separation results are shown in Fig. 14. It can be seen that the background noise can be effectively removed by the proposed method.

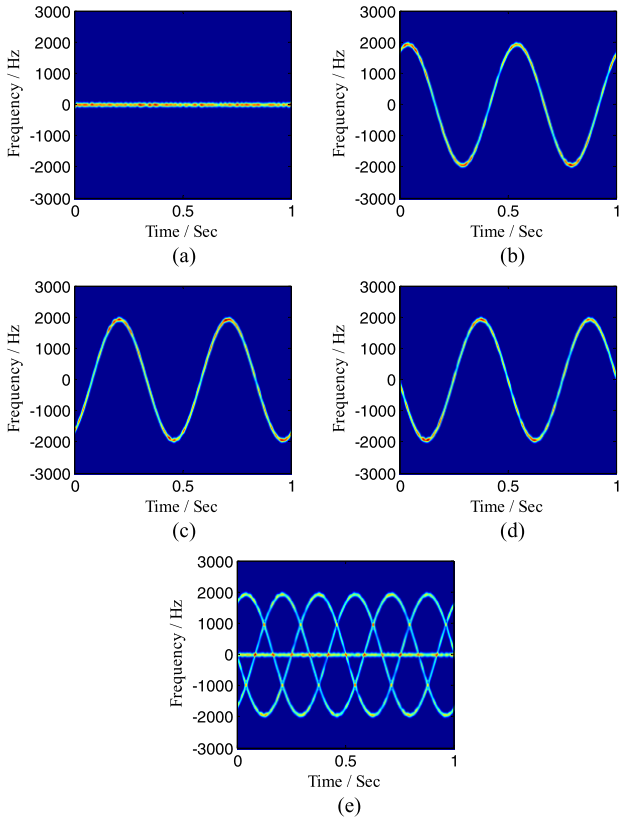

Fig. 12. Component separation for the m-D signal in Fig. 11 by ICCD. (a)∼(d) The obtained individual components. (e) The sum of these obtained components (SNR = 12.75 dB).

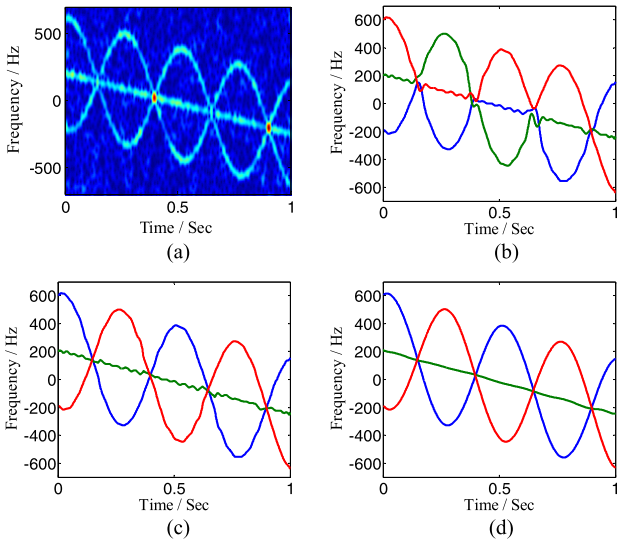

Fig. 13. Simulated m-D signal of a tumbling target and the IF extraction results. (a) TFR of the noisy m-D signal (SNR = 0 dB). (b) Result by ridge detection. (c) Result by RPRG. (d) Result after smoothing the curves in (c).

The third example is a pure coning target rotating with an angular velocity of 4π rad/s around an axis which intersects with the axis of symmetry. We also consider three scattering points, i.e., two rotating points and one fixed point located at the conic node. The m-D signal (SNR = 0 dB) and the corresponding IF extraction results are illustrated in Fig. 15.

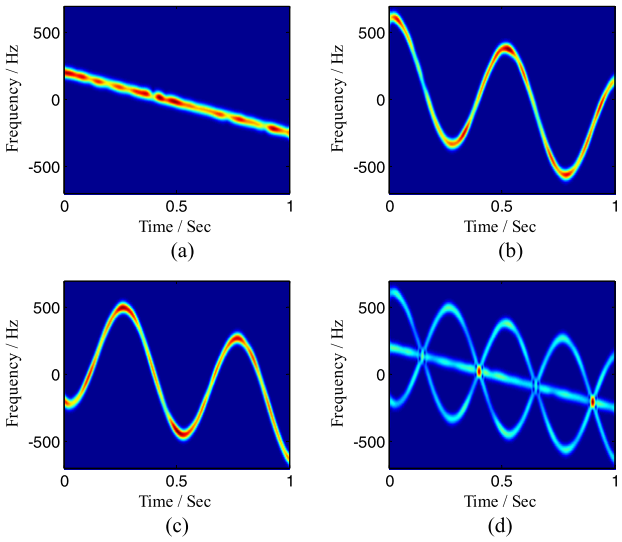

Fig. 14. Component separation for the m-D signal in Fig. 13 by ICCD. (a)∼(c) The obtained individual components. (d) The sum of these obtained components (SNR = 14.23 dB).

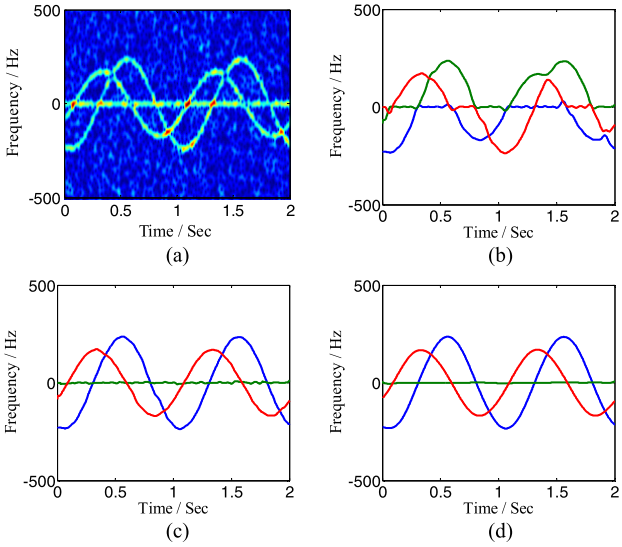

Fig. 15. Simulated m-D signal of a coning target and the IF extraction results. (a) TFR of the noisy m-D signal (SNR = 0 dB). (b) Result by ridge detection. (c) Result by RPRG. (d) Result after smoothing the curves in (c).

The component separation results for the coning target are shown in Fig. 16. It can be seen that the proposed method can effectively separate these overlapped components and remarkably increase the SNR of the signal.

The traditional T-F filtering technique is often used to separate non-stationary signals [19]–[21], [28]. For comparison, we also consider to separate the m-D signals above by the T-F filter. The T-F filtering method mainly includes three steps: first, the considered non-stationary signal is transformed (or demodulated) into the baseband using the estimated IF; then a low-pass filter is employed to extract the baseband signal; finally, the target non-stationary signal is recovered by modulating the baseband signal with the same estimated IF. Herein the IFs (regarded as the center frequencies of the

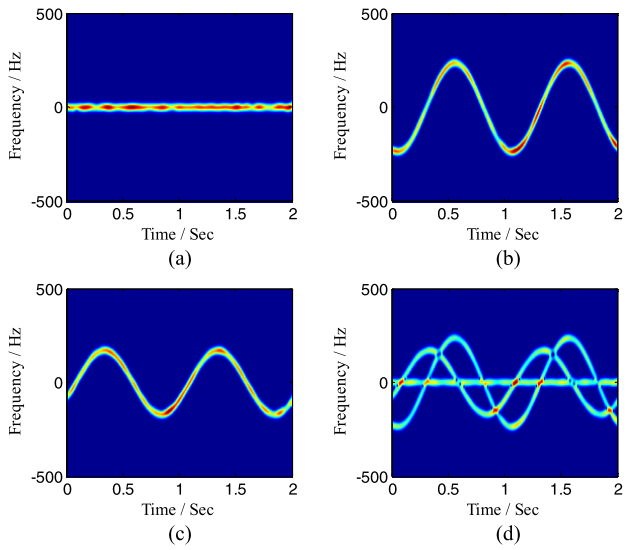

Fig. 16. Component separation for the m-D signal in Fig. 15 by ICCD. (a)∼(c) The obtained individual components. (d) The sum of these obtained components (SNR = 16.14 dB).

TABLE I

SNRs OF THE RECONSTRUCTED M-D SIGNALS OF DIFFERENT TARGETS BY DIFFERENT METHODS WITH 0 AND 10 dB NOISE

	0 dB		10 dB	
	T-F filter	ICCD	T-F filter	ICCD
Rotating	11.99 dB	12.75 dB	17.18 dB	23.09 dB
Tumbling	12.24 dB	14.23 dB	17.50 dB	24.12 dB
Coning	14.01 dB	16.14 dB	16.93 dB	25.89 dB

T-F filter) of the m-D signals are still estimated by the proposed RPRG algorithm. The component separation is carried out at two SNR levels, i.e., 0 dB and 10 dB. We calculate the SNRs of the sum of the extracted components as listed Table I where the bandwidth of the T-F filter and the ICCD are both set to 1% of the sampling frequency. It shows that, at 0 dB, the advantage of the ICCD over the T-F filter is less obvious. It is because, in a low SNR, the results are dominated by the input bandwidth (of the filter or ICCD) which determines the proportion of removed noise. On the other hand, when the input SNR is increased (e.g., 10 dB or higher), the performance of the ICCD will significantly outperform that of the T-F filter as shown in Table I. It is because that the T-F filter will split other components near the intersections and thus result in information loss (e.g., see Fig. 3(d)) when extracting a certain signal component whose IF intersects with those of others. Conversely, the ICCD has much higher accuracy of reconstructing overlapped components. The simulation results indicate that the proposed method has potential to separate m-D signals with severely overlapped components.

B. Experiment Results

In this subsection, the proposed method will be applied to separate an experimental m-D signal from rotating targets.

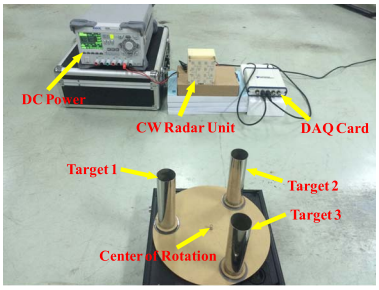

Fig. 17. Experimental setup for detecting motions of three rotating targets with CW radar.

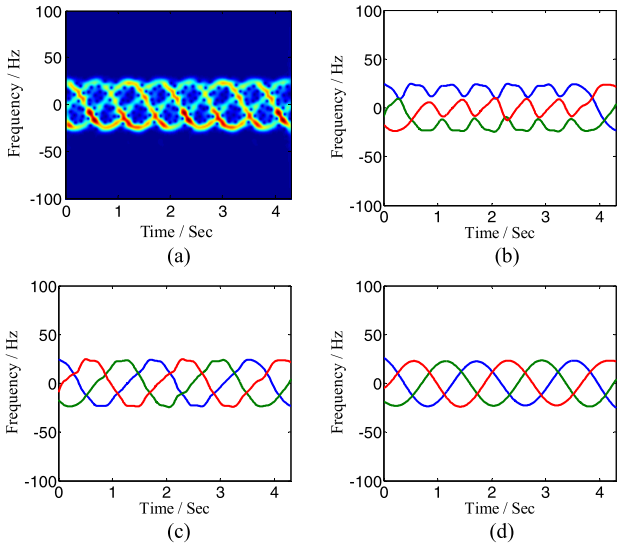

Fig. 18. Experimental m-D data and the IF extraction results. (a) TFR of the experimental m-D signal. (b) Result by ridge detection. (c) Result by RPRG. (d) Result after smoothing the curves in (c).

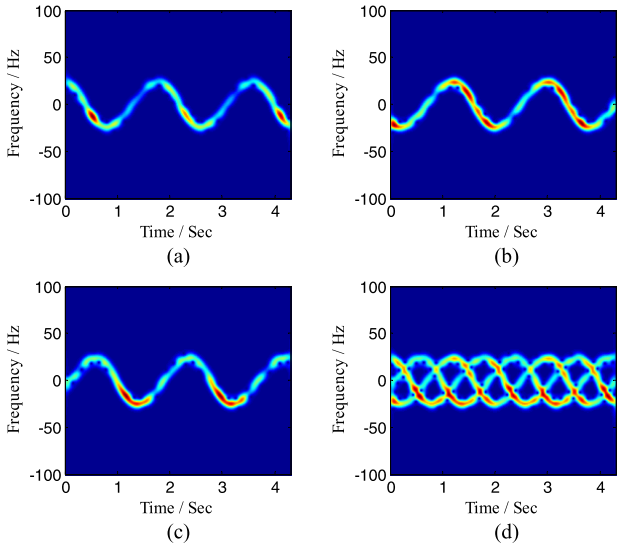

Fig. 19. Component separation for the experimental signal in Fig. 18. (a)∼(c) The obtained individual components. (d) The sum of these obtained components.

A continuous-wave (CW) radar with a frequency of 10.5 GHz is used to detect the motion of the targets. In this experiment, three metallic cylinders are fixed on a turntable which rotates with the speed of 33 rpm, as shown in Fig. 17. The experimental setup is inspired by that in [43]. The three cylinders are regarding as three rotating targets in this paper.

The obtained m-D data is shown in Fig. 18(a). It can be seen that the m-D signatures of the experimental signal are sinusoidal curves (similar to that in Fig. 11(a)) but there exists serious interference between the signal components in the TFR. Clearly, the ridge detection method cannot properly discriminate these components (see Fig. 18(b)). The proposed RPRG algorithm effectively tracks the correct T-F patterns of these severely overlapped components (see Fig. 18(c)). The obtained ridge paths can be further smoothed to reduce the interference of clutters, as illustrated in Fig. 18(d). The component separation results are shown in Fig. 19. It can be observed that all the components are successfully extracted and clutters are effectively removed. One can further accurately extract m-D signatures from the obtained individual components, which will be the topic of our future work.

V. Conclusion

In this paper, we proposed a novel method which combines the RPRG algorithm with the ICCD to separate severely overlapped components. The proposed RPRG algorithm first detects the ridge curves of all the components and then regroups the obtained ridges according to their variation rates. The RPRG is fully non-parametric and can adapt to different situations. Comparing with traditional ridge extraction methods, the RPRG can deal with signals with overlapped components. As far as we know, few methods can address this challenging issue. Having obtained the IF information by RPRG, component separation can be achieved by ICCD. To show the effectiveness of the proposed method, we first analyzed some simulated m-D signals induced by rotating, tumbling, and coning targets. Then, the method was also used to separate an experimental m-D signal. The simulation and experiment results indicate that the method is effective for a wide range of signals composed of overlapped components.

It should be pointed out that the proposed RPRG algorithm is in essence a post-processing method. Therefore, the performance of the RPRG relies on the quality of the detected ridge curves (i.e., Step 1 in Section III-B). For simplicity, in this paper, we use Algorithm 1 to detect the ridges from the TFR generated by STFT. In a very noisy environment, one should choose more robust ridge detectors such as those in [44] and [45]. To improve the accuracy of the IF estimation, one can also choose TFRs with higher resolution such as the one generated by S-method [27] or synchrosqueezing transform [10]. In the future, we will investigate other practical applications related to radar fields using the method.

References

[1] V. C. Chen, F. Li, S.-S. Ho, and H. Wechsler, "Micro-Doppler effect in radar: Phenomenon, model, and simulation study," *IEEE Trans. Aerosp. Electron. Syst.*, vol. 42, no. 1, pp. 2–21, Jan. 2006.

[2] Z. Feng, M. Liang, and F. Chu, "Recent advances in time–frequency analysis methods for machinery fault diagnosis: A review with application examples," *Mech. Syst. Signal Process.*, vol. 38, no. 1, pp. 165–205, Jul. 2013.

[3] S. K. Hadjidimitriou and L. J. Hadjileontiadis, "Toward an EEG-based recognition of music liking using time-frequency analysis," *IEEE Trans. Biomed. Eng.*, vol. 59, no. 12, pp. 3498–3510, Dec. 2012.

[4] Z. K. Peng, G. Meng, F. L. Chu, Z. Q. Lang, W. M. Zhang, and Y. Yang, "Polynomial chirplet transform with application to instantaneous frequency estimation," *IEEE Trans. Instrum. Meas.*, vol. 60, no. 9, pp. 3222–3229, Sep. 2011.

[5] Y. Yang, Z. K. Peng, X. J. Dong, W. M. Zhang, and G. Meng, "General parameterized time-frequency transform," *IEEE Trans. Signal Process.*, vol. 62, no. 11, pp. 2751–2764, Jun. 2014.

[6] T. Sakamoto, T. Sato, P. J. Aubry, and A. G. Yarovoy, "Texture-based automatic separation of echoes from distributed moving targets in UWB radar signals," *IEEE Trans. Geosci. Remote Sens.*, vol. 53, no. 1, pp. 352–361, Jan. 2015.

[7] X. Shi, F. Zhou, M. Tao, and Z. Zhang, "Human movements separation based on principle component analysis," *IEEE Sensors J.*, vol. 16, no. 7, pp. 2017–2027, Apr. 2016.

[8] N. E. Huang *et al.*, "The empirical mode decomposition and the Hilbert spectrum for nonlinear and non-stationary time series analysis," *Proc. Roy. Soc. London Ser. A, Math., Phys. Eng. Sci.*, vol. 454, no. 1971, pp. 903–995, Mar. 1998.

[9] J. S. Smith, "The local mean decomposition and its application to EEG perception data," *J. Roy. Soc. Interface*, vol. 2, no. 5, pp. 443–454, 2005.

[10] I. Daubechies, J. Lu, and H.-T. Wu, "Synchrosqueezed wavelet transforms: An empirical mode decomposition-like tool," *Appl. Computat. Harmon. Anal.*, vol. 30, no. 2, pp. 243–261, Mar. 2011.

[11] J. Gilles, "Empirical wavelet transform," *IEEE Trans. Signal Process.*, vol. 61, no. 16, pp. 3999–4010, Aug. 2013.

[12] K. Dragomiretskiy and D. Zosso, "Variational mode decomposition," *IEEE Trans. Signal Process.*, vol. 62, no. 3, pp. 531–544, Feb. 2014.

[13] S. G. Mallat and Z. Zhang, "Matching pursuits with time-frequency dictionaries," *IEEE Trans. Signal Process.*, vol. 41, no. 12, pp. 3397–3415, Dec. 1993.

[14] T. Y. Hou and Z. Shi, "Data-driven time-frequency analysis," *Appl. Computat. Harmon. Anal.*, vol. 35, no. 2, pp. 284–308, Sep. 2013.

[15] S. Chen, Z. Peng, Y. Yang, X. Dong, and W. Zhang, "Intrinsic chirp component decomposition by using Fourier series representation," *Signal Process.*, vol. 137, pp. 319–327, Aug. 2017.

[16] Y. Ding and J. Tang, "Micro-Doppler trajectory estimation of pedestrians using a continuous-wave radar," *IEEE Trans. Geosci. Remote Sens.*, vol. 52, no. 9, pp. 5807–5819, Sep. 2014.

[17] S. Chen, Y. Yang, K. Wei, X. Dong, Z. Peng, and W. Zhang, "Time-varying frequency-modulated component extraction based on parameterized demodulation and singular value decomposition," *IEEE Trans. Instrum. Meas.*, vol. 65, no. 2, pp. 276–285, Feb. 2016.

[18] Y. Yang, Z. Peng, X. Dong, W. Zhang, and G. Meng, "Application of parameterized time-frequency analysis on multicomponent frequency modulated signals," *IEEE Trans. Instrum. Meas.*, vol. 63, no. 12, pp. 3169–3180, Dec. 2014.

[19] Y. Yang, X. Dong, Z. Peng, W. Zhang, and G. Meng, "Component extraction for non-stationary multi-component signal using parameterized de-chirping and band-pass filter," *IEEE Signal Process. Lett.*, vol. 22, no. 9, pp. 1373–1377, Sep. 2015.

[20] C. Ioana, C. Gervaise, Y. Stéphan, and J. I. Mars, "Analysis of underwater mammal vocalisations using time–frequency-phase tracker," *Appl. Acoust.*, vol. 71, no. 11, pp. 1070–1080, Nov. 2010.

[21] C. Ioana, A. Jarrot, C. Gervaise, Y. Stéphan, and A. Quinquis, "Localization in underwater dispersive channels using the time–frequency-phase continuity of signals," *IEEE Trans. Signal Process.*, vol. 58, no. 8, pp. 4093–4107, Aug. 2010.

[22] S. Chen, X. Dong, Y. Yang, W. Zhang, Z. Peng, and G. Meng, "Chirplet path fusion for the analysis of time-varying frequency-modulated signals," *IEEE Trans. Ind. Electron.*, vol. 64, no. 2, pp. 1370–1380, Feb. 2017.

[23] L. Stanković, M. Daković, T. Thayaparan, and V. Popović-Bugarin, "Inverse radon transform–based micro-Doppler analysis from a reduced set of observations," *IEEE Trans. Aerosp. Electron. Syst.*, vol. 51, no. 2, pp. 1155–1169, Apr. 2015.

[24] Q. Zhang, T. S. Yeo, H. S. Tan, and Y. Luo, "Imaging of a moving target with rotating parts based on the hough transform," *IEEE Trans. Geosci. Remote Sens.*, vol. 46, no. 1, pp. 291–299, Jan. 2008.

[25] I. Djurović and L. Stanković, "An algorithm for the Wigner distribution based instantaneous frequency estimation in a high noise environment," *Signal Process.*, vol. 84, no. 3, pp. 631–643, Mar. 2004.

[26] H. Zhang, G. Bi, S. G. Razul, and C. M. S. See, "Robust time-varying filtering and separation of some nonstationary signals in low SNR environments," *Signal Process.*, vol. 106, pp. 141–158, Jan. 2015.

[27] T. Thayaparan, L. Stanković, and I. Djurović, "Micro-Doppler-based target detection and feature extraction in indoor and outdoor environments," *J. Franklin Inst.*, vol. 345, no. 6, pp. 700–722, Sep. 2008.

[28] P. Li, D.-C. Wang, and L. Wang, "Separation of micro-Doppler signals based on time frequency filter and Viterbi algorithm," *Signal, Image Video Process.*, vol. 7, no. 3, pp. 593–605, May 2013.

[29] L. Stanković, T. Thayaparan, M. Daković, and V. Popović-Bugarin, "Micro-Doppler removal in the radar imaging analysis," *IEEE Trans. Aerosp. Electron. Syst.*, vol. 49, no. 2, pp. 1234–1250, Apr. 2013.

[30] S. Stanković, I. Djurović, and T. Thayaparan, "Separation of target rigid body and micro-Doppler effects in ISAR imaging," *IEEE Trans. Aerosp. Electron. Syst.*, vol. 42, no. 4, pp. 1496–1506, Oct. 2006.

[31] L. Stanković, I. Orović, S. Stanković, and M. Amin, "Compressive sensing based separation of nonstationary and stationary signals overlapping in time-frequency," *IEEE Trans. Signal Process.*, vol. 61, no. 18, pp. 4562–4572, Sep. 2013.

[32] P. Suresh, T. Thayaparan, T. Obulesu, and K. Venkataramaniah, "Extracting micro-Doppler radar signatures from rotating targets using Fourier–Bessel transform and time–frequency analysis," *IEEE Trans. Geosci. Remote Sens.*, vol. 52, no. 6, pp. 3204–3210, Jun. 2014.

[33] X. Bai, M. Xing, F. Zhou, G. Lu, and Z. Bao, "Imaging of micromotion targets with rotating parts based on empirical-mode decomposition," *IEEE Trans. Geosci. Remote Sens.*, vol. 46, no. 11, pp. 3514–3523, Nov. 2008.

[34] B. Yuan, Z. Chen, and S. Xu, "Micro-Doppler analysis and separation based on complex local mean decomposition for aircraft with fast-rotating parts in ISAR imaging," *IEEE Trans. Geosci. Remote Sens.*, vol. 52, no. 2, pp. 1285–1298, Feb. 2014.

[35] H. Zhang, G. Bi, W. Yang, S. G. Razul, and C. M. S. See, "IF estimation of FM signals based on time-frequency image," *IEEE Trans. Aerosp. Electron. Syst.*, vol. 51, no. 1, pp. 326–343, Jan. 2015.

[36] P. C. Hansen and D. P. O'Leary, "The use of the L-curve in the regularization of discrete ill-posed problems," *SIAM J. Sci. Comput.*, vol. 14, no. 6, pp. 1487–1503, Nov. 1993.

[37] E. Sejdic, I. Djurović, and L. Stanković, "Quantitative performance analysis of scalogram as instantaneous frequency estimator," *IEEE Trans. Signal Process.*, vol. 56, no. 8, pp. 3837–3845, Aug. 2008.

[38] S. Meignen, T. Oberlin, and S. McLaughlin, "A new algorithm for multicomponent signals analysis based on synchrosqueezing:W ith an application to signal sampling and denoising," *IEEE Trans. Signal Process.*, vol. 60, no. 11, pp. 5787–5798, Nov. 2012.

[39] N. A. Khan and B. Boashash, "Instantaneous frequency estimation of multicomponent nonstationary signals using multiview time-frequency distributions based on the adaptive fractional spectrogram," *IEEE Signal Process. Lett.*, vol. 20, no. 2, pp. 157–160, Feb. 2013.

[40] B. Barkat and K. Abed-Meraim, "Algorithms for blind components separation and extraction from the time-frequency distribution of their mixture," *EURASIP J. Appl. Signal Process.*, vol. 13, pp. 2025–2033, Jan. 2004.

[41] L. Du, Y. Ma, B. Wang, and H. Liu, "Noise-robust classification of ground moving targets based on time-frequency feature from micro-Doppler signature," *IEEE Sensors J.*, vol. 14, no. 8, pp. 2672–2682, Aug. 2014.

[42] L. Du, B. Wang, Y. Li, and H. Liu, "Robust classification scheme for airplane targets with low resolution radar based on EMD-CLEAN feature extraction method," *IEEE Sensors J.*, vol. 13, no. 12, pp. 4648–4662, Dec. 2013.

[43] M. Anabuki *et al.*, "Ultrawideband radar imaging using adaptive array and Doppler separation," *IEEE Trans. Aerosp. Electron. Syst.*, vol. 53, no. 1, pp. 190–200, Feb. 2017.

[44] M. Brajović, V. Popović-Bugarin, I. Djurović, and S. Djukanović, "Post-processing of time-frequency representations in instantaneous frequency estimation based on ant colony optimization," *Signal Process.*, vol. 138, pp. 195–210, Sep. 2017.

[45] D. Iatsenko, P. V. McClintock, and A. Stefanovska, "Extraction of instantaneous frequencies from ridges in time–frequency representations of signals," *Signal Process.*, vol. 125, pp. 290–303, Aug. 2016.

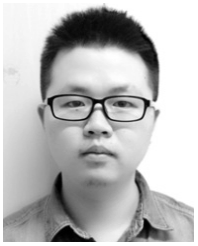

Shiqian Chen received the B.S. degree in mechanical engineering from Sichuan University, Chengdu, China, in 2014. He is currently pursuing the Ph.D. degree in mechanical engineering with Shanghai Jiao Tong University, Shanghai, China.

He is currently with the State Key Laboratory of Mechanical System and Vibration, Shanghai Jiao Tong University. His current research interests include time–frequency analysis and machine health diagnosis.

Xingjian Dong received the B.S. degree in aircraft design engineering and the M.S. degree in solid mechanics from Northwestern Polytechnical University, Xi'an, China, in 1999 and 2002, respectively, and the Ph.D. degree in mechanical engineering from Shanghai Jiao Tong University, Shanghai, China, in 2006.

He is currently an Associate Professor with the State Key Laboratory of Mechanical System and Vibration, Shanghai Jiao Tong University. His current research interests include vibration analysis, smart structures, and the fatigue analysis of structures.

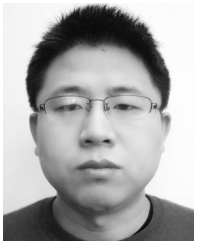

Guanpei Xing received the B.S. and M.S. degrees from the School of Mechatronics Engineering, Harbin Institute of Technology, Harbin, China, in 2003 and 2005, respectively.

He is currently a Senior Engineer with the Shanghai Aerospace Electronic Technology Institute. His research interest is radar signal processing.

Zhike Peng received the B.Sc. and Ph.D. degrees from Tsinghua University, Beijing, China, in 1998 and 2002, respectively.

He was a Research Associate with The City University of Hong Kong, Hong Kong, from 2003 to 2004, and a Research Officer with Cranfield University, Cranfield, U.K. He was with The University of Sheffield, Sheffield, U.K., for four years. He is currently a Cheung Kong Chair Professor with the State Key Laboratory of Mechanical System and Vibration, Shanghai Jiao Tong University, Shanghai, China. His current research interests include nonlinear vibration, signal processing and condition monitoring, and fault diagnosis for machines and structures.

Wenming Zhang (M'10) received the B.S. degree in mechanical engineering and the M.S. degree in mechanical design and theories from Southern Yangtze University, Wuxi, China, in 2000 and 2003, respectively, and the Ph.D. degree in mechanical engineering from Shanghai Jiao Tong University, Shanghai, China, in 2006.

He is currently a Professor with the State Key Laboratory of Mechanical System and Vibration, School of Mechanical Engineering, Shanghai Jiao Tong University. He has been involved in the dynamics and control for micro/nanoelectromechanical systems (MEMS/NEMS). His current research interests include nonlinear dynamics and chaos control, nonlinear vibration and control, coupled parametrically excited microresonators, and the reliability analysis and assessment for MEMS/NEMS applications.

Guang Meng received the Ph.D. degree from Northwestern Polytechnical University, Xi'an, China, in 1988.

In 1993, he was a Professor and the Director of the Vibration Engineering Institute, Northwestern Polytechnical University. From 1989 to 1993, he was also a Research Assistant with Texas A&M University, College Station, an Alexander von Humboldt Fellow with Technical University Berlin, Berlin, Germany, and a Research Fellow with New South Wales University, Sydney, Australia. From 2000 to 2008, he was with Shanghai Jiao Tong University, Shanghai, China, as the Cheung Kong Chair Professor, the Associate Dean, and the Dean of the School of Mechanical Engineering. He is currently a Professor with the State Key Laboratory of Mechanical System and Vibration, Shanghai Jiao Tong University. His research interests include the dynamics and vibration control of mechanical systems, nonlinear vibration, and microelectromechanical systems.